Eur. Phys. J. B **53**, 449–454 (2006)
DOI: 10.1140/epjb/e2006-00411-7

THE EUROPEAN PHYSICAL JOURNAL B

Optical bistability via tunable Fano-type interference in asymmetric semiconductor quantum wells

J.H. Li[a] and X.X. Yang

Department of Physics, Huazhong University of Science and Technology, Wuhan 430074, P.R. China

Received 15 August 2006 / Received in final form 29 September 2006
Published online 17 November 2006 –

Abstract. We analyze hybrid absorptive-dispersive optical bistability (OB) behavior via tunable Fano-type interference based on intersubband transitions in asymmetric double quantum wells (QWs) driven coherently by a probe laser field by means of a unidirectional ring cavity. We show that OB can be controlled efficiently by tuning the energy splitting of the two excited states (the coupling strength of the tunnelling), the Fano-type interference, and the frequency detuning. The influence of the electronic cooperation parameter on the OB behavior is also discussed. This investigation may be used for optimizing and controlling the optical switching process in the QW solid-state system, which is much more practical than that in atomic system because of its flexible design and the controllable interference strength.

PACS. 78.67.De Quantum wells – 42.65.Pc Optical bistability, multistability, and switching, including local field effects – 42.50.Gy Effects of atomic coherence on propagation, absorption, and amplification of light

1 Introducion

Optical bistability (OB) has been extensively studied both experimentally and theoretically in two-level atomic systems due to its wide applications such as optical transistors, memory elements and all optical switches [1,2]. The OB in three-level atomic systems confined optical ring cavity has also been studied theoretically [3] and experimentally [4]. It has been shown that the field-induced transparency and quantum interference effects could significantly decrease the OB threshold [5]. The phase fluctuation effects [6] and the effects of squeezed state fields [7–9] on the optical bistability have subsequently studied. It has been found that the OB could appear for small cooperation parameters due to the present of squeezed vacuum field [9].

In recent years there have been much interests in the effect of spontaneously generated coherence (SGC) on the dynamics [10], the amplification without population inversion [11], the disappearance of the dark state due to SGC in Λ-type atomic systems [12] and the enhanced index of refraction without absorption [13–17]. It also affects on the optical bistability behavior in three-level atomic systems such as its threshold [18,19] and the shape of the bistable hysteresis cycle [20]. However, the existence of SGC or vacuum-induced coherence (VIC) requires that two close-lying levels be near-degenerate and that the atomic dipole moments be non-orthogonal for the atoms in free space. Unfortunately, it is very difficult, if not impossible, to find a real atomic system with SGC or VIC because the rigorous conditions of near-degenerate levels and non-orthogonal dipole matrix elements are hard to be simultaneously satisfied. As a result, few experiments have been performed to observe these interesting phenomena based on SGC/VIC. It is thus desirable to put forward new schemes without the SGC effect to realize the OB and/or optical multistability (OM) to overcome the above mentioned difficulties.

It should be noted that similar phenomena involving quantum coherence and interference in QW systems [21–41] have also attracted great attention due to the potentially important applications in optoelectronics and solid-state quantum information science. For example, it has been shown that they can lead to coherently controlled photoncurrent generation [32], electron intersubband transitions [33,34], electromagnetically induced transparency (EIT) [35], and gain without inversion [26–28]. Devices based on intersubband transitions in semiconductor QW structures have many inherent advantages, such as large electric dipole moments due to the small effective electron mass, high nonlinear optical coefficients, and a great flexibility in device design by choosing the materials and structure dimensions. Furthermore, the transition energies, dipoles, and symmetries can be engineered as desired. The implementation of EIT in semiconductor-based devices is very attractive from a viewpoint of applications. It is worth pointing out that Joshi and Xiao recently analyze the OB behavior in a semiconductor quantum well

[a] e-mail: huajia_li@163.com

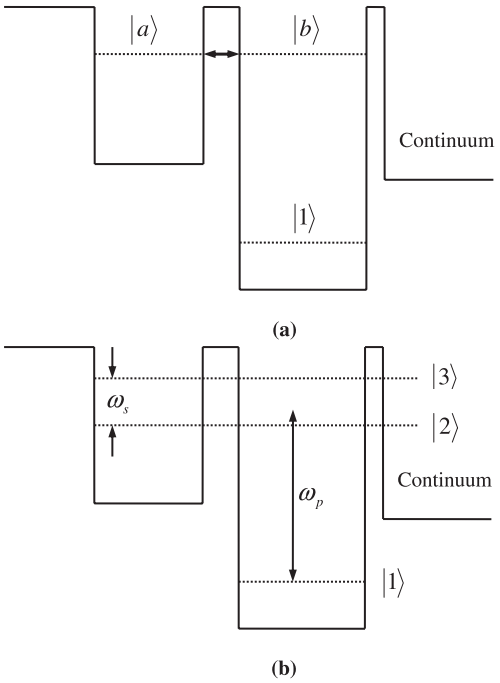

Fig. 1. (a) Energy level diagram of a double quantum well structure. It consists of two quantum wells and a collector region separated by thin tunnelling barriers. (a) Subband $|a\rangle$ of the shallow well is resonant with the second subband $|b\rangle$ of the deep well. (b) Due to the strong coherent coupling via the thin barrier, the levels split into a doublet $|2\rangle$ and $|3\rangle$, which are coupled to a continuum by a thin tunnelling barrier adjacent to the deep well. Also shown in (b) are the splitting between the two upper levels ω_s (given by the coherent coupling strength) and the weak probe laser ω_p.

that interacts with two electromagnetic fields, a strong field and a weak field, and show that the threshold for switching to upper branch of the bistable curve can be reduced due to the presence of quantum interference [40].

In this paper, we demonstrate, for the first time, the controllability of OB via tuning the coupling strength of the tunnelling, the Fano-type interference, and the frequency detuning in asymmetric double quantum well structures using intersubband transitions by applications of a coherent probe laser field. The nature of OB and OM in our scheme is a hybrid type that combines both absorptive and dispersive types.

Figure 1 shows the double quantum well scheme under consideration. It consists of two quantum wells that are separated by a narrow barrier. The first subband ($|a\rangle$) of the shallow well is resonant with the second subband ($|b\rangle$) of the deep well (see Fig. 1a), and due to the strong coherent coupling via the thin barrier, the levels split into a doublet, levels $|2\rangle$ and $|3\rangle$ (see Fig. 1b), which arise from the mixing of the states $|a\rangle$ and $|b\rangle$, under the exactly resonant conditions, $|2\rangle = (|a\rangle - |b\rangle)/\sqrt{2}$, $|3\rangle = (|a\rangle + |b\rangle)/\sqrt{2}$. The splitting ω_s on resonance is given by the coupling strength and can be controlled by adjusting the height and width of the tunnelling barrier with applied bias voltage [24].

We assume that a weak probe field of amplitude E_p and angular frequency ω_p is used to illuminate the QW system, and interacts on both the transitions $|1\rangle \leftrightarrow |2\rangle$ and $|1\rangle \leftrightarrow |3\rangle$ simultaneously with the respective Rabi frequencies $\Omega_{p1} = \mu_{31}E_p/2\hbar$ and $\Omega_{p2} = \mu_{21}E_p/2\hbar$ with μ_{31} and μ_{21} being the intersubband dipole moments of the respective transition.

In the present analysis we use the following conditions: (1) the electron sheet density of the quantum well structure is such that electron-electron effects have very small influence in our results. Therefore, the effects of electron-electron interactions are not included in our study; (2) we assume that all subbands have the same effective mass. Using the density-matrix formalism we begin to describe the dynamic response of the three-level QW system under study. By adopting the standard approach (this method has described quantitatively the results of several experimental papers [22,24,28,30,34] and has been used in several theoretical papers [25,27,36,38,40]), under the electro-dipole and rotating-wave approximations we can easily obtain the time-dependent density matrix equations of motion as follows:

$$
\begin{aligned}
\dot{\rho}_{22} &= -\gamma_2\rho_{22} + i\Omega_{p2}\left(\rho_{12} - \rho_{21}\right) - \frac{\kappa}{2}\left(\rho_{23} + \rho_{32}\right),\\
\dot{\rho}_{33} &= -\gamma_3\rho_{33} + i\Omega_{p1}\left(\rho_{13} - \rho_{31}\right) - \frac{\kappa}{2}\left(\rho_{23} + \rho_{32}\right),\\
\dot{\rho}_{12} &= -\frac{\gamma_{21}}{2}\rho_{12} + i\left(\Delta_p - \frac{\omega_s}{2}\right)\rho_{12}\\
&\quad + i\Omega_{p2}\left(\rho_{22} - \rho_{11}\right) + i\Omega_{p1}\rho_{32} - \frac{\kappa}{2}\rho_{13},\\
\dot{\rho}_{13} &= -\frac{\gamma_{31}}{2}\rho_{13} + i\left(\Delta_p + \frac{\omega_s}{2}\right)\rho_{13}\\
&\quad + i\Omega_{p1}\left(\rho_{33} - \rho_{11}\right) + i\Omega_{p2}\rho_{23} - \frac{\kappa}{2}\rho_{12},\\
\dot{\rho}_{23} &= -\frac{\gamma_{32}}{2}\rho_{23} + i\omega_s\rho_{23} + i\Omega_{p2}\rho_{13}\\
&\quad - i\Omega_{p1}\rho_{21} - \frac{\kappa}{2}\left(\rho_{22} + \rho_{33}\right),
\end{aligned}
\tag{1}
$$

together with $\rho_{ij} = \rho^*_{ji}$ and the carrier conservation condition $\sum_{j=1}^{3}\rho_{jj} = 1$. Here $\omega_s = E_3 - E_2$ is the energy splitting between the upper levels, given by the coherent coupling strength of the tunnelling. $\Delta_p = \omega_0 - \omega_p$ is the detuning between the frequency of the probe laser and the average transition frequency $\omega_0 = (\omega_2 + \omega_3)/2$. Above the dots denote the derivative with respect to time t and Rabi frequencies Ω_{pi} $(i = 1, 2)$ are assumed real. The population decay rates and dephasing decay rates are added phenomenologically in the above density matrix equations [30,37]. The population decay rates for subband $|i\rangle$, denoted by γ_i, are due primarily to longitudinal optical (LO) phonon emission events at low temperature. The total decay rates γ_{ij} $(i \neq j)$ are given by $\gamma_{21} = \gamma_2 + \gamma_{21}^{dph}$, $\gamma_{31} = \gamma_3 + \gamma_{31}^{dph}$, and $\gamma_{32} = \gamma_2 + \gamma_3 + \gamma_{32}^{dph}$, where γ_{ij}^{dph}, determined by electron-electron, interface roughness, and phonon scattering processes, is the dephasing decay rate of the quantum coherence of the $|i\rangle \leftrightarrow |j\rangle$ transition. $\kappa = \sqrt{\gamma_2\gamma_3}$ represents the mutual coupling of states $|2\rangle$ and $|3\rangle$ via the LO phonon decay, it describes the process in which a phonon is emitted by subband $|2\rangle$ and is

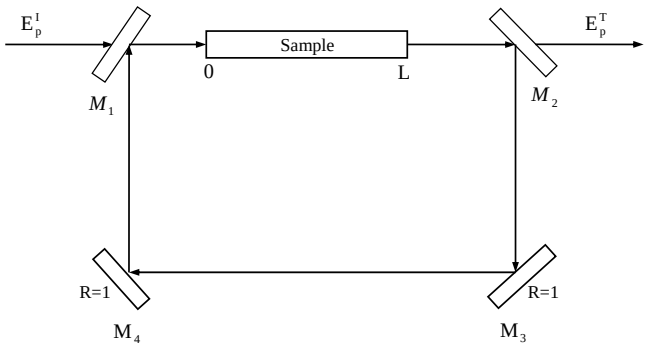

Fig. 2. Unidirectional ring cavity with a QW sample of length L, E_p^I and E_p^T are the incident and the transmitted field, respectively.

recaptured by subband $|3\rangle$. These mutual coupling terms can be obtained if tunnelling is present, e.g., through an additional barrier next to the deeper well [24,25]. As mentioned above, levels $|2\rangle$ and $|3\rangle$ are both the superpositions of the resonant states $|a\rangle$ and $|b\rangle$. Because the latter (subband $|b\rangle$) are strongly coupled to a continuum via a thin barrier, the decay from state $|b\rangle$ to the continuum inevitably results in these two dependent decay pathways: from the excited doublet to the common continuum. That is to say, the two decay pathways are related: the decay from one of the excited doublets can strongly affect the neighbouring transition, resulting in the interference characterized by those mutual coupling terms. Such interference is similar to the "decay-induced" coherence in atomic systems with two closely lying energy states. Note that, in the following numerical calculations the choices of the parameters are based on experimental results from reference [24].

The most interesting parameter, defined by the ratio $\epsilon = \kappa/\sqrt{\gamma_{21}\gamma_{31}}$, is used to assess the strength or quality of the interference [24], where the limit values $\epsilon = 0$ and $\epsilon = 1$ correspond, respectively, to no interference (negligible coupling between $|2\rangle$ and $|3\rangle$) and perfect interference (no dephasing). Without loss of generality, taking $\mu_{21} = \mu_{31} = \mu$, thus we have the relationships $\Omega_{p1} = \Omega_{p2} = \Omega_p$. Now, we put the QW sample in a unidirectional ring cavity (see Fig. 2). For simplicity, we assume that mirror 3 and 4 have 100% reflectivity, and the intensity reflection and transmission coefficient of mirrors 1 and 2 are R and T (with $R + T = 1$), respectively.

The total electromagnetic field can be written as $E = E_p e^{-i\omega_p t} + c.c.$, where the probe field E_p circulates in the ring cavity. Then under slowly varying envelope approximation, the dynamic response of the probe field is governed by Maxwell's equation

$$\frac{\partial E_p}{\partial t} + c\frac{\partial E_p}{\partial z} = i\frac{\omega_p}{2\varepsilon_0}P(\omega_p), \tag{2}$$

where c and ε_0 is the light speed and permittivity of free space respectively. $P(\omega_p)$ is the slowly oscillating term of the induced polarization in both the intersubband transitions $|1\rangle \leftrightarrow |2\rangle$ and $|1\rangle \leftrightarrow |3\rangle$, and is determined by $P(\omega_p) = N\mu(\rho_{21} + \rho_{31})$, where N is the electron density in the conduction band of the QW.

We consider the field equation (2) in the steady-state case. Setting the time derivative in equation (2) equal to zero for the steady state, we can obtain the field amplitude as follows:

$$\frac{\partial E_p}{\partial z} = i\frac{N\omega_p\mu}{2c\varepsilon_0}(\rho_{21} + \rho_{31}). \tag{3}$$

For a perfectly tuned ring cavity, in the steady state limit, the boundary conditions impose the following conditions between the incident field E_p^I and the transmitted field E_p^T

$$E_p(L) = E_p^T/\sqrt{T}, \tag{4a}$$

$$E_p(0) = \sqrt{T}E_p^I + RE_p(L), \tag{4b}$$

where L is the length of the QW sample, and the second term on the right-hand side of equation (4b) describes a feedback mechanism due to the mirror, which is essential to give rise to bistability, that is to say, no bistability can occur if $R = 0$.

In the mean-field limit [42], using the boundary conditions equation (4) and normalizing the fields by letting $y = \frac{\mu E_p^I}{\hbar\sqrt{T}}$ and $x = \frac{\mu E_p^T}{2\hbar\sqrt{T}}$, we can get input-output relationship:

$$y = 2x - iC(\rho_{21}(x) + \rho_{31}(x)), \tag{5}$$

where $C = \frac{N\omega_p L\mu^2}{2\hbar\varepsilon_0 cT}$ is the electronic cooperation parameter. It is worthwhile pointing out that the second term on the right-hand side of equation (5) is vital for optical bistability and multistability to take place.

We set the time derivatives $\partial\rho_{ij}/\partial t = 0$ $(i, j = 1, 2, 3)$ in the above density matrix equation (1) for the steady state, and solve the corresponding density matrix equation together with the coupled field equation (5) via nice Matlab codes, then we can arrive at the steady-state solutions.

In the following we present a few numerical results for the steady state of the output field intensity versus the input filed intensity with different corresponding parameters, as illustrated in Figures 3–7. First of all, we will analyze how the energy splitting of the two excited states which is given by the coupling strength of the tunnelling modifies the bistable behavior, while keeping all other parameters fixed. Figure 3 demonstrates the dependence of the optical bistability on the energy splitting ω_s, and for the purpose of gaining an insight into the physical origin Figure 4 shows the dependence of the probe absorption on the frequency detunings Δ_p. It can be easily seen from Figure 3 that increasing the splitting on resonance leads to a significant decreasing of the bistable threshold y_{th}. The reason can be qualitatively explained as follows. By applying an increasingly intense resonant tunnelling through a thin barrier, the absorption for the probe field on the intersubband transitions $|1\rangle \leftrightarrow |2\rangle$ and $|1\rangle \leftrightarrow |3\rangle$ of the electronic medium can be reduced dramatically as shown in

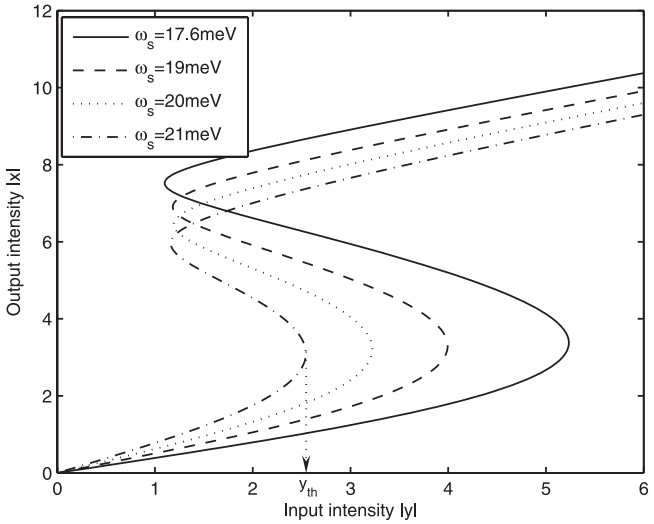

Fig. 3. Output intensity $|x|$ versus input intensity $|y|$ for different splitting ω_s. Other parameters are $C = 200$ meV, $\Delta_p = 0$ meV, $\gamma_2 = 5.6$ meV, $\gamma_3 = 7.0$ meV, $\gamma_{21}^{dph} = 1.5$ meV, $\gamma_{31}^{dph} = 2.3$ meV, and $\gamma_{32}^{dph} = 1.9$ meV.

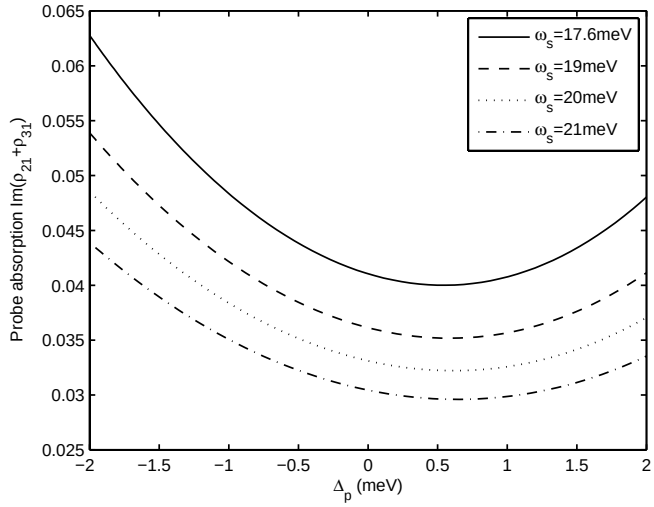

Fig. 4. Probe absorption $\mathrm{Im}(\rho_{21} + \rho_{31})$ as a function of probe detuning Δ_p with different splitting ω_s. The parameters are the same as in Figure 3 except for $\Omega_p = 2$ meV.

Figure 4, which makes the cavity field easier to reach saturation. This might be useful to control the threshold value and the hysteresis cycle width of the bistable curve simply by adjusting the splitting. As mentioned above, the splitting on resonance is given by the coupling strength and can be controlled by adjusting the height and width of the tunnelling barrier. Therefore, the behavior of OB can be tuned by appropriately adjusting the tunnelling barrier.

The effects of the strength or quality of the interference on OB can be clearly seen from Figure 5. From this figure, we can observe reduction of threshold as we go from $\epsilon = 0.46$ (dash-dotted curve) to $\epsilon = 0.77$ (solid curve), and the region of OB becomes narrowed. As a result, we can achieve optimally the desired bistable curve via properly tuning the Fano interference. In order to have a better

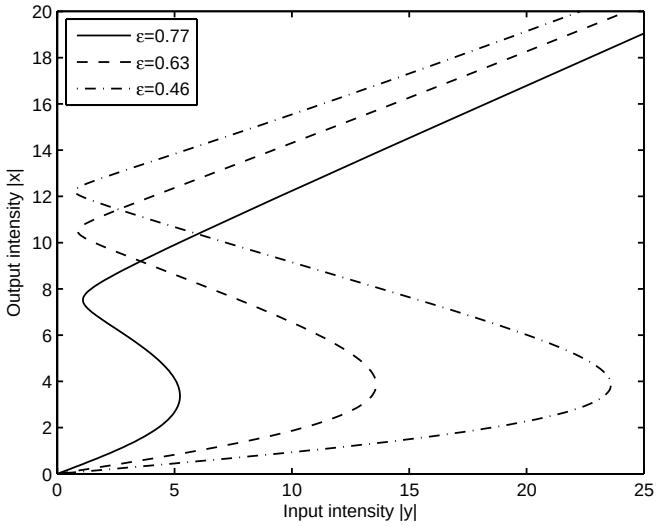

Fig. 5. Output intensity $|x|$ versus input intensity $|y|$ for different interference strengths ϵ. Solid curve ($\epsilon = 0.77$): $\gamma_{21}^{dph} = 1.5$ meV, $\gamma_{31}^{dph} = 2.3$ meV, and $\gamma_{32}^{dph} = 1.9$ meV; dashed curve ($\epsilon = 0.63$): $\gamma_{21}^{dph} = 3.0$ meV, $\gamma_{31}^{dph} = 4.6$ meV, and $\gamma_{32}^{dph} = 3.8$ meV; dash-dotted curve ($\epsilon = 0.46$): $\gamma_{21}^{dph} = 6.0$ meV, $\gamma_{31}^{dph} = 9.2$ meV, and $\gamma_{32}^{dph} = 7.6$ meV. Other parameters are $\omega_s = 17.6$ meV, $C = 200$ meV, $\Delta_p = 0$ meV, $\gamma_2 = 5.6$ meV, and $\gamma_3 = 7.0$ meV.

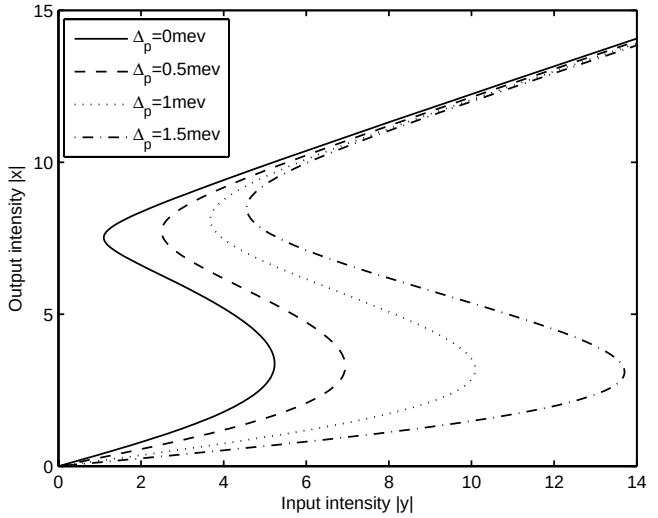

Fig. 6. Output intensity $|x|$ versus input intensity $|y|$ for different values of Δ_p. Other parameters are $\omega_s = 17.6$ meV, $C = 200$ meV, $\gamma_2 = 5.6$ meV, $\gamma_3 = 7.0$ meV, $\gamma_{21}^{dph} = 1.5$ meV, $\gamma_{31}^{dph} = 2.3$ meV, and $\gamma_{32}^{dph} = 1.9$ meV.

idea about how the bistable threshold value changes with the frequency detuning of the probe laser, in Figure 6 we plot the output amplitude as a function of input amplitude for different values of the frequency detuning of the probe field, i.e., Δ_p. With increasing Δ_p from 0 to 1.5 meV, the threshold of OB increases progressively and the area of the hysteresis cycle becomes wider.

In Figure 7, we display the behavior of OB with different values of the cooperation parameter C. It is easy

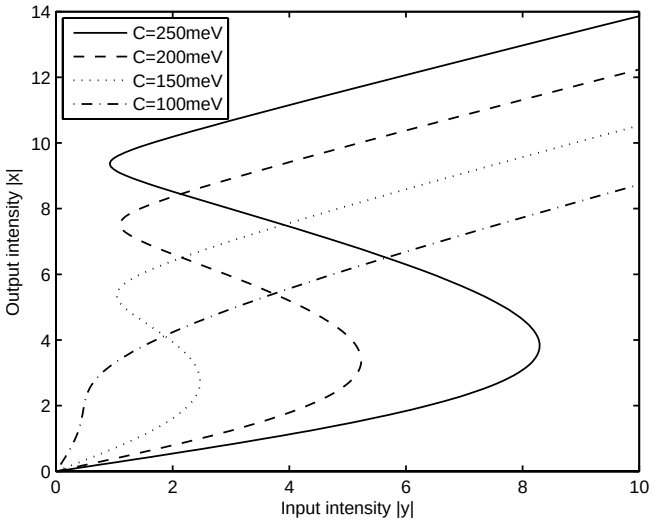

Fig. 7. Output intensity $|x|$ versus input intensity $|y|$ for different values of C. Other parameters are $\omega_s = 17.6$ meV, $\Delta_p = 0$ meV, $\gamma_2 = 5.6$ meV, $\gamma_3 = 7.0$ meV, $\gamma_{21}^{dph} = 1.5$ meV, $\gamma_{31}^{dph} = 2.3$ meV, and $\gamma_{32}^{dph} = 1.9$ meV.

to see from Figure 7 that, when the cooperation parameter C becomes small, i.e., the number density of electrons in the sample decreases, the threshold of OB is reduced drastically and OB tends to disappear. When C is equal to 100 meV or much smaller, there is no OB. However, OB is obviously seen when the cooperation parameter C is large. From the term $C = N\omega_p L\mu^2/2\hbar\varepsilon_0 cT$, we can see that the cooperation parameter C is directly proportional to the electron number density N. So the enhancement in the absorption of the sample as the number density of electrons increases could account for the raise of the threshold intensity with respect to the cooperation parameter C.

In conclusion, we have illustrated the OB behaviors in a three-subband QW system driven by a coherent probe field inside a unidirectional ring cavity. We find that the energy splitting of the two excited states (the coupling strength of the tunnelling), the Fano-type interference as well as the cooperation parameters can affect the OB behavior dramatically, which can be used to manipulate efficiently the bistable threshold intensity and the hysteresis loop. Our calculations also provide a guideline for the optimal design of QW systems to achieve very fast and low-threshold all-optical switches [4] in such semiconductor systems which is much more practical than that in atomic system because of its flexible design and the controllable interference strength. Lastly, we point out that the OB comes essentially from the Kerr nonlinearity and hence solitons could form in those systems of demonstrating OB behaviors [43].

The research is supported in part by the National Natural Science Foundation of China (Grant Nos. 10575040, 60478029, 10634060 and 90503010) and by National Basic Research Program of China under Contract No. 2005CB724508. We would like to thank Professor Ying Wu for helpful discussion and his encouragement.

References

1. See, for example, a review by L.A. Lugiato, *Theory of Optical Bistability, in Progress in Optics*, edited by E. Wolf (North-Holland, Amsterdam, 1984), Vol. 21, p. 71, and references therein
2. H.M. Gibbs, S.L. McCall, T.N.C. Venkatesan, Phys. Rev. Lett. **36**, 1135 (1976); A.T. Rosenberger, L.A. Orozco, H.J. Kimble, Phys. Rev. A **28**, 2569 (1983); L.A. Orozco et al., Phys. Rev. A **39**, 1235 (1989)
3. D.F. Wall, P. Zoller, Opt. Commun. **34**, 260 (1980)
4. A. Joshi, M. Xiao, Phys. Rev. Lett. **91**, 143904 (2003); A. Joshi, A. Brown, H. Wang, M. Xiao, Phys. Rev. A **67**, 041801(R) (2003); A. Joshi, W. Yang, M. Xiao, Phys. Rev. A **70**, 041802(R) (2004); A. Joshi, W. Yang, M. Xiao, Opt. Lett. **30**, 905 (2005); H. Chang, H. Wu, C. Xie, H. Wang, Phys. Rev. Lett. **93**, 213901 (2004)
5. W. Harshawardhan, G.S. Agarwal, Phys. Rev. A **53**, 1812 (1996)
6. X. Hu, Z. Xu, J. Opt. B: Quantum Semiclass. Opt. **3**, 35 (2001)
7. S. Singh, J. Rai, C.M. Bowden, A. Postan, Phys. Rev. A **45**, 5160 (1992)
8. P. Galatola, L.A. Lugiato, M.G. Porreca, P. Tombesi, Opt. Commun. **81**, 175 (1991)
9. Z. Chen, C. Du, S. Gong, Z. Xu, Phys. Lett. A **259**, 15 (1999)
10. A. Joshi, W. Yang, M. Xiao, Phys. Lett. A **325**, 30 (2004)
11. O. Kocharovskaya, Y.A. Khanin, JETP Lett. **48**, 630 (1988); A. Imamoğlu, J.E. Field, S.E. Harris, Phys. Rev. Lett. **66**, 1154 (1991)
12. J. Javanainen, Europhys. Lett. **17**, 407 (1992)
13. M.O. Scully, Phys. Rev. Lett. **67**, 1855 (1991)
14. S.E. Harris, J.E. Field, A. Kasapi, Phys. Rev. A **46**, R29 (1992)
15. R.R. Moseley, S. Shepherd, D.J. Fulton, B.D. Sinclair, M.H. Dunn, Phys. Rev. Lett. **74**, 670 (1995)
16. A.S. Zibrov, M.D. Lukin, L. Hollberg, D.E. Nikonov, M.O. Scully, H.G. Robinson, V.L. Velichansky, Phys. Rev. Lett. **76**, 3935 (1996)
17. M. Fleischhauer, C.H. Keitel, M.O. Scully, C. Su, B.T. Ulrich, S.Y. Zhu, Phys. Rev. A **46**, 1468 (1992)
18. A. Joshi, W. Yang, M. Xiao, Phys. Rev. A **68**, 015806 (2003)
19. A. Joshi, W. Yang, M. Xiao, Phys. Lett. A **315**, 203 (2003)
20. D. Cheng, C. Liu, S. Gong, Phys. Lett. A **332**, 244 (2004)
21. J. Faist, C. Sirtori, F. Capasso, S.N.G. Chu, L.N. Pfeiffer, K.W. West, Opt. Lett. **21**, 985 (1996)
22. J. Faist, F. Capasso, C. Sirtori, K. West, L.N. Pfeiffer, Nature **390**, 589 (1997)
23. J. Faist, F. Capasso, C. Sirtori, D.L. Sivco, A.L. Hutchinson, S.N.G. Chu, A.Y. Cho, Appl. Phys. Lett. **65**, 94 (1994)
24. H. Schmidt, K.L. Campman, A.C. Gossard, A. Imamoğlu, Appl. Phys. Lett. **70**, 3455 (1997)
25. H. Schmidt, A. Imamoğlu, Opt. Commun. **131**, 333 (1996)
26. A. Imamoğlu, R.J. Ram, Opt. Lett. **19**, 1744 (1994)
27. C.R. Lee, Y.C. Li, F.K. Men, C.H. Pao, Y.C. Tsai, J.F. Wang, Appl. Phys. Lett. **86**, 201112 (2004)

28. M.D. Frogley, J.F. Dynes, M. Beck, J. Faist, C.C. Phillips, Nature Mater. **5**, 175 (2006)
29. C. Gmachl, Nature Mater. **5**, 169 (2006)
30. G.B. Serapiglia, E. Paspalakis, C. Sirtori, K.L. Vodopyanov, C.C. Phillips, Phys. Rev. Lett. **84**, 1019 (2000)
31. T. Li, H. Wang, N.H. Kwong, R. Binder, Opt. Express **11**, 3298 (2003); X.X. Yang, Z.W. Li, Y. Wu, Phys. Lett. A **340**, 320 (2005); Y. Wu, J. Saldana, Y. Zhu, Phys. Rev. A **67**, 013811 (2003); Y. Wu, L. Wen, Y. Zhu, Opt. Lett. **28**, 631 (2003)
32. R. Atanasov, A. Haché, J.L.P. Hughes, H.M. van Driel, J.E. Sipe, Phys. Rev. Lett. **76**, 1703 (1996)
33. W. Pötz, Physica E (Amsterdam) **7**, 159 (2000); W. Pötz, Phys. Rev. B **71**, 125331 (2005)
34. T. Müller, W. Parz, G. Strasser, K. Unterrainer, Phys. Rev. B **70**, 155324 (2004); T. Müller, W. Parz, G. Strasser, K. Unterrainer, Appl. Phys. Lett. **84**, 64 (2004); T. Müller, R. Bratschitsch, G. Strasser, K. Unterrainer, Appl. Phys. Lett. **79**, 2755 (2001)
35. D.E. Nikonov, A. Imamoğlu, M.O. Scully, Phys. Rev. B **59**, 12212 (1999); M. Phillips, H. Wang, Opt. Lett. **28**, 831 (2003); L. Silvestri et al., Eur. Phys. J. B **27**, 89 (2002)
36. J.F. Dynes, M.D. Frogley, J. Rodger, C.C. Phillips, Phys. Rev. B **72**, 085323 (2005); J.F. Dynes, E. Paspalakis, Phys. Rev. B **73**, 233305 (2006)
37. J.F. Dynes, M.D. Frogley, M. Beck, J. Faist, C.C. Phillips, Phys. Rev. Lett. **94**, 157403 (2005)
38. J.H. Wu, J.Y. Gao, J.H. Xu, L. Silvestri, M. Artoni, G.C. La Rocca, F. Bassani, Phys. Rev. Lett. **95**, 057401 (2005); J.H. Wu, J.Y. Gao, J.H. Xu, L. Silvestri, M. Artoni, G.C. La Rocca, F. Bassani, Phys. Rev. A **73**, 053818 (2006)
39. P.C. Ku, F. Sedgwick, C.J. Chang-Hasnain, P. Palinginis, T. Li, H. Wang, S.W. Chang, S.L. Chuang, Opt. Lett. **29**, 2291 (2004); S. Sarkar, Y. Guo, H. Wang, Opt. Express **14**, 2845 (2006); S.F. Yelin, P.R. Hemmer, Phys. Rev. A **66**, 013803 (2002)
40. A. Joshi, M. Xiao, Appl. Phys. B: Lasers Opt. **79**, 65 (2004)
41. C.Z. Ning, Phys. Rev. Lett. **93**, 187403 (2004); A. Liu, C.Z. Ning, Appl. Phys. Lett. **75**, 1207 (1999)
42. R. Bonifacio, L.A. Lugiato, Lett. Nuovo Cimento **21**, 505 (1978)
43. Y. Wu, Phys. Rev. A **71**, 053820 (2005); Y. Wu, L. Deng, Opt. Lett. **29**, 2064 (2004); Y. Wu, L. Deng, Phys. Rev. Lett. **93**, 143904 (2004)